

Title: Strong damping-like spin-orbit torque and tunable Dzyaloshinskii-Moriya interaction generated by low-resistivity Pd_{1-x}Pt_x alloys

*Lijun Zhu, *Kemal Sobotkiewich, Xin Ma, Xiaoqin Li, Daniel. C. Ralph, Robert A. Buhrman**

Dr. L. J. Zhu, Prof. R. A. Buhrman

Cornell University, Ithaca, NY 14850, USA

Email: lz442@cornell.edu; rab8@cornell.edu

K. Sobotkiewich, Dr. X. Ma, Prof. X. Li

Department of Physics, Center for Complex Quantum Systems, The University of Texas at Austin,
Austin, Texas 78712, USA

Prof. D. C. Ralph

Cornell University, Ithaca, NY 14850, USA

Kavli Institute at Cornell, Ithaca, New York 14853, USA

Abstract: Despite their great promise for providing a pathway for very efficient and fast manipulation of magnetization at the nanoscale, spin-orbit torque (SOT) operations are currently energy inefficient due to a low damping-like SOT efficiency per unit current bias, and/or the very high resistivity of the spin Hall materials. Here, we report an advantageous spin Hall material, $\text{Pd}_{1-x}\text{Pt}_x$, which combines a low resistivity with a giant spin Hall effect as evidenced through the use of three independent SOT ferromagnetic detectors. The optimal $\text{Pd}_{0.25}\text{Pt}_{0.75}$ alloy has a giant internal spin Hall ratio of >0.47 (damping-like SOT efficiency of ~ 0.26 for all three ferromagnets) and a low resistivity of $\sim 57.5 \mu\Omega \text{ cm}$ at 4 nm thickness. Moreover, we find the Dzyaloshinskii-Moriya interaction (DMI), the key ingredient for the manipulation of chiral spin arrangements (e.g. magnetic skyrmions and chiral domain walls), is considerably strong at the $\text{Pd}_{1-x}\text{Pt}_x/\text{Fe}_{0.6}\text{Co}_{0.2}\text{B}_{0.2}$ interface when compared to that at $\text{Ta}/\text{Fe}_{0.6}\text{Co}_{0.2}\text{B}_{0.2}$ or $\text{W}/\text{Fe}_{0.6}\text{Co}_{0.2}\text{B}_{0.2}$ interfaces and can be tuned by a factor of 5 through control of the interfacial spin-orbital coupling via the heavy metal composition. This work establishes a very effective spin current generator that combines a notably high energy efficiency with a very strong and tunable DMI for advanced chiral spintronics and spin torque applications.

1. Introduction

Current-induced spin-orbit torques (SOTs) in heavy metal/ferromagnet (HM/FM) systems have promise for more efficient and faster electrical manipulation of magnetization at the nanoscale than magnetic field and conventional spin-transfer torque.^[1-7] The damping-like SOT generated by the *bulk* spin Hall effect (SHE) of the HMs is of particular interest in exciting magnetization dynamics at microwave and terahertz frequencies,^[1,2] driving skyrmion and chiral domain wall displacement^[3,4] or switching the magnetization of thin film nanomagnets.^[5-7] Despite extensive efforts,^[1-9] the energy efficiency of present SOT operations is still limited by a relatively low damping-like SOT efficiency (ζ_{DL})^[6] and/or a high resistivity (ρ_{xx}) of the spin Hall materials^[8,9] (see Table I). When ρ_{xx} of the spin Hall material is comparable to or larger than that of the metallic FM being manipulated, the detrimental shunting of applied current through the FM layer will be significant (see Supporting Information). Another important ingredient for spin-orbit coupling (SOC) phenomena is the Dzyaloshinskii-Moriya interaction (DMI) at HM/FM interfaces due to the combination of the broken inversion symmetry and *interfacial* spin-orbit coupling (SOC).^[10] The interfacial DMI is a short-range antisymmetric exchange interaction that can promote chiral spin alignments, e.g. in magnetic skyrmions and chiral domain walls.^[3,4] The sign and magnitude of the interfacial DMI influence the direction and velocity of a chiral spin texture movement driven by damping-like SOT. For a perpendicularly magnetized multi-domain HM/FM structure, the interfacial DMI represents an obstacle for SOT switching of magnetization via a thermally-activated reversal domain nucleation and domain wall depinning process,^[5] because it requires an external field or its equivalent that is larger than the DMI field applied along the bias current direction in order to switch the magnetization. This requirement leads to additional complexity in the design and implementation of SOT devices. The DMI may also play a role in the sub-ns micromagnetic dynamics that are critical to the reliable switching of nanoscale SOT-magnetic random access memories (MRAMs).^[11,12] Therefore, exploration of new, more efficient HM spin Hall materials and new routes to tune the DMI strength

continues to be of significant scientific interest and technological importance.

Pt is a particularly interesting spin Hall material due to its giant intrinsic spin Hall conductivity (σ_{SH}) arising from the Berry curvature of its band structure.^[13,14] However, the reported values of ζ_{DL} for Pt/FM systems are generally low, e.g. ~ 0.07 in Pt/Ni₈₁Fe₁₉ bilayers ($\rho_{xx} \approx 20 \mu\Omega \text{ cm}$),^[15] ~ 0.12 in Pt/Co bilayers ($\rho_{xx} \approx 30 \mu\Omega \text{ cm}$).^[16] Recently, the introduction of impurities^[17] or disorder^[18] has been found to raise ρ_{xx} and to degrade σ_{SH} of Pt (the band structure) at the same time. A good trade-off between ρ_{xx} and σ_{SH} can enhance ζ_{DL} of Pt to some degree (< 0.16 ^[18]) because $\zeta_{\text{DL}} = T_{\text{int}}(2e/\hbar)\sigma_{\text{SH}}\rho_{xx}$ for the intrinsic SHE mechanism. Alloying Pt with Au was recently found to be more effective than introducing impurities and disorders in enhancing the ζ_{DL} as it allows significant increase in ρ_{xx} without degrading σ_{SH} in the fcc alloy with the optimized composition.^[14]

In this work, based on direct spin-torque measurements using perpendicular magnetic anisotropy (PMA) Co, in-plane magnetic anisotropy (IMA) Co, and IMA Fe_{0.6}Co_{0.2}B_{0.2} as the FM detectors, we report an effective magnification of the damping-like SOT efficiency and internal spin Hall conductivity (i.e. ζ_{DL} and σ_{SH}) in Pd_{1-x}Pt_x alloy. A large ζ_{DL} of ≈ 0.26 and a giant σ_{SH} of $1.1 \times 10^6 \hbar/2e \Omega^{-1} \text{ m}^{-1}$ was obtained in Pd_{0.25}Pt_{0.75} which still has a relatively low resistivity of $\sim 57.5 \mu\Omega \text{ cm}$, making Pd_{0.25}Pt_{0.75} a strong and particularly advantageous spin Hall material from the viewpoint of energy efficiency of spintronic applications. We also find from Brillouin light scattering (BLS) measurements that the DMI at Pd_{1-x}Pt_x/Fe_{0.6}Co_{0.2}B_{0.2} interfaces is both considerably strong and variable over a wide range (5 \times) by controlling the interfacial SOC via the HM composition.

2. Results and Discussions

2.1. Sample details

We sputter deposited Pd_{1-x}Pt_x d /Co t bilayers and Pd_{1-x}Pt_x d /Fe_{0.6}Co_{0.2}B_{0.2} t bilayers (here t and d are thicknesses in nm) with different Pt concentration ($x = 0, 0.25, 0.5, 0.75, \text{ and } 1$) onto oxidized Si substrates (**Figure 1a**). X-ray diffraction θ - 2θ patterns (**Figure S1**, Supporting Information) show that

the fcc Pd_{1-x}Pt_x (111) diffraction peak gradually shifts with increasing x , affirming the uniform alloying of the two elements. For this study, the Co layers were wedges with thickness varying between 0.75-1.4 nm for $x = 1$ and between 0.64-0.94 nm for $x \leq 0.75$ across the wafer to enable the study of both PMA and IMA Pd_{1-x}Pt_x/Co devices. For Pd_{1-x}Pt_x/Co bilayers, the saturation magnetization (M_s) varies between 1450 and 1700 emu/cm³ for different x , indicative of an enhancement due to a magnetic proximity effect at the interface,^[19] which, however, should not degrade ζ_{DL} as is discussed in Ref. [20,21]. M_s for the Pd_{1-x}Pt_x/Fe_{0.6}Co_{0.2}B_{0.2} bilayers remains almost constant with x , ~ 1200 emu/cm³. The stacks were patterned into $5 \times 60 \mu\text{m}^2$ Hall bars by ultraviolet photolithography and ion milling. The magnetic bilayer samples were further patterned into $5 \times 60 \mu\text{m}^2$ Hall bars for measuring SOTs by out-of-plane (PMA bilayers) and in-plane (IMA bilayers) harmonic response measurements^[22,23] (see **Figure S2** and **S3** in Supporting Information for more details).

2.2. Tuning the SHE by composition

We determined ρ_{xx} for 4 nm Pd_{1-x}Pt_x layers by subtracting the sheet conductance of reference stacks Ta 1/Co t /MgO 2/Ta 1.5 and Ta 1/ Fe_{0.6}Co_{0.2}B_{0.2} t /MgO 2/Ta 1.5 from that of our samples containing the Pd_{1-x}Pt_x layer. As plotted in **Figure 1b**, ρ_{xx} for 4 nm Pd_{1-x}Pt_x layers varies between 37.0 and 57.6 $\mu\Omega$ cm for different x . The alloys with $0.25 \leq x \leq 0.75$ have greater ρ_{xx} than pure Pt or Pd for all three FM cases, which we attribute to enhanced electron scattering in the chemically disordered alloys. At a given x for the different FM samples, there are only small differences in ρ_{xx} likely due to modest differences in interfacial scattering. **Figure 1c** shows the x dependence of ζ_{DL} generated by 4 nm Pd_{1-x}Pt_x for PMA Co ($t = 0.64$ or 0.75), IMA Co ($t = 0.94$ or 1.4), and IMA Fe_{0.6}Co_{0.2}B_{0.2} ($t = 2.8$) detectors. Here $\zeta_{DL} = 2e\mu_0 M_s t H_{DL} / \hbar j_e$, where μ_0 , M_s , and H_{DL} are the permeability of vacuum, saturation magnetization, and the damping-like SOT effective field. For all three FM cases, ζ_{DL} increases quickly from ~ 0.07 at $x = 0$ (pure Pd) to the peak value of ~ 0.26 at $x = 0.75$, and then drops to ~ 0.20 at $x = 1$ (pure Pt). The consistent peak behavior of ζ_{DL} at $x \approx 0.75$ is attributable to the non-monotonic x

dependence of ρ_{xx} (Figure 1b) and the giant apparent spin Hall conductivity $\sigma_{\text{SH}}^* = T_{\text{int}}\sigma_{\text{SH}} = (\hbar/2e)\zeta_{\text{DL}}/\rho_{xx}$ for $x \geq 0.75$. As seen in Figure 1d, σ_{SH}^* for 4 nm Pd_{1-x}Pt_x increases monotonically with x and exhibits a weak peak at $x \approx 0.75$ for the PMA case. Interestingly, the x dependence is *functionally* similar to the predicted behavior for the intrinsic spin Hall conductivities of Pd_{1-x}Pt_x alloys in a recent *ab initio* calculation,^[14] although as we will discuss below the actual spin Hall conductivities for Pd_{1-x}Pt_x are much larger than indicated by the *ab initio* results in Ref. [14] once the degradation of T_{int} by spin backflow (SBF) and spin memory loss (SML) at the FM interfaces^[24] is taken into account. Finally, we point out that for each FM case, σ_{SH}^* of the 4 nm Pd_{0.25}Pt_{0.75} is comparable with that of pure Pt, i.e. $(4.6\text{-}5.1) \times 10^5 \hbar/2e \Omega^{-1} \text{ m}^{-1}$. This is distinct from the case of introducing Hf impurities into Pt,^[17] where σ_{SH}^* is degraded by $> 25\%$ after the Hf impurity concentration reaches 12.5%. Another interesting observation is that σ_{SH}^* for each x is overall *slightly* different for the three FM detectors, i.e. $\sigma_{\text{SH}}^* (\text{Fe}_{0.6}\text{Co}_{0.2}\text{B}_{0.2} \text{ IMA}) > \sigma_{\text{SH}}^* (\text{Co IMA}) > \sigma_{\text{SH}}^* (\text{Co PMA})$. This difference is attributable in part to the Co thickness in the PMA sample being less than its spin dephasing length (~ 1 nm), because of which the spin current is not completely absorbed after going through the FM layer,^[16] and in part, we speculate, to differences in SBF and SML at the different interfaces. The maximum $\zeta_{\text{DL}} \approx 0.26$ for 4 nm Pd_{0.25}Pt_{0.75} is comparable to that of highly resistive β -W ($\approx 300 \mu\Omega \text{ cm}$),^[8] while ρ_{xx} is as low as $\sim 57.5 \mu\Omega \text{ cm}$, less than one-fourth of that of β -W with similar thickness.^[8] It is interesting to notice that ζ_{DL} for 4 nm Pd_{0.25}Pt_{0.75} is even slightly smaller than ~ 0.30 for 4 nm Au_{0.25}Pt_{0.75} ($\approx 80 \mu\Omega \text{ cm}$)^[14] due to its low ρ_{xx} despite that their similar σ_{SH}^* . We note also that $\zeta_{\text{DL}} \approx 0.2$ for the PMA Pt 4/Co 0.75 bilayers ($\rho_{xx} \approx 51 \mu\Omega \text{ cm}$, see Figure 1b) is larger than ~ 0.12 (~ 0.08) as previously reported for Pt/Co (Pt/Ni₈₁Fe₁₉) bilayers where ρ_{xx} was lower, as small as 30 (20) $\mu\Omega \text{ cm}$.^[14,16] This difference in ρ_x and hence in ζ_{DL} is most likely due to differences in film growth protocols. Finally our result of $\zeta_{\text{DL}} = 0.07$ for Pd is comparable with that reported for Pd/Co/AlO_x (~ 0.06).^[25]

Now we consider possible reasons for the absence of the strong SHE and enhanced damping-like SOT efficiency in two previous reports.^[26,27] Zhou *et al.*^[26] reported from a spin-torque ferromagnetic

resonance (ST-FMR) study that the spin Hall angle (θ_{SH}) of $\text{Pd}_{1-x}\text{Pt}_x$ was enhanced to ~ 0.05 in the composition range $0.5 \leq x \leq 0.8$ compared to -0.005 for Pd and 0.04 for Pt. In another inverse SHE/spin pumping work,^[27] θ_{SH} of $\text{Pd}_{1-x}\text{Pt}_x$ was found to be ~ 0.17 at $x \approx 0.8$, which is larger than 0.045 in Pd to 0.125 in Pt. Despite the similar trends as we observe, the two experiments seem to considerably underestimate the SHE strength of the alloys. We note that the ST-FMR analysis ignored any influence of SBF, SML, field-like SOT, and the measurement artifacts (e.g. a strong dependence of the SOT efficiency on the microwave frequency). Meanwhile, both spin diffusion length (λ_s) and ρ_{xx} of the HMs, which are crucial for the analysis of an inverse SHE experiment, were assumed to be independent of the HM thickness, which is however an invalid assumption as discussed below and in Ref. [28].

2.3. Spin backflow and internal spin Hall effect

The spin diffusion length (λ_s) and spin conductance $1/\lambda_s\rho_{xx}$ are two key parameters for the theoretical understanding of a spin Hall material, for determining the spin Hall ratio (θ_{SH}) of a HM via an inverse SHE experiment, and for optimizing the SOT effectiveness of the material. We determined $1/\lambda_s\rho_{xx}$ for $\text{Pd}_{0.25}\text{Pt}_{0.75}$, the optimal composition for the largest ζ_{DL} (**Figure 1c**) by studying H_{DL} and ζ_{DL} for a series of $\text{Pd}_{0.25}\text{Pt}_{0.75}$ d/Co 0.64 bilayers as a function of d . As plotted in **Figure 2a**, H_{DL}/E initially increases quickly and then gradually saturates with increasing d , consistent with the spin diffusion behavior expected by the SHE model. ζ_{DL} , however, first increases as d increases from 2 nm, peaks at $d = 3-4$ nm, and then drops gradually as d further increases (**Figure 2b**). This is a direct consequence of the combination of the decreasing ρ_{xx} with d as interfacial scattering becomes less dominant (**Figure 2c**) and the rapid and then saturating increase in σ_{SH}^* (the black squares in **Figure 2d**) as d increases up to and then beyond the HM λ_s . Overall, the average resistivity ρ_{xx} of the $\text{Pd}_{0.25}\text{Pt}_{0.75}$ layers drops from $86.8 \mu\Omega \text{ cm}$ at $d = 2$ nm to $37.4 \mu\Omega \text{ cm}$ at $d = 8$ nm. Such an interesting peak behavior of ζ_{DL} and the strong thickness dependence of ρ_{xx} were not observed in $\text{Au}_{0.25}\text{Pt}_{0.75}$ where the mean-free path was very short. [14]

If we assume the usual case where the interfacial spin mixing conductance $G^{\uparrow} \approx \text{Re}G^{\uparrow}$, a negligible SML at the HM/FM interface, and a ρ_{xx} -independent λ_s , both λ_s and σ_{SH} can be obtained by [28]

$$\sigma_{\text{SH}}^* = \sigma_{\text{SH}} (1 - \text{sech}(d/\lambda_s)) (1 + \tanh(d/\lambda_s) / 2\lambda_s \rho_{xx} \text{Re}G^{\uparrow})^{-1} \quad [1]$$

However, this equation is not valid for Pd_{0.25}Pt_{0.75} as ρ_{xx} varies strongly with d and λ_s is not a constant if the Elliot-Yafet spin scattering mechanism dominates, where $\lambda_s \propto 1/\rho_{xx}$. Considering this effect, we can use the ‘‘rescaling’’ method introduced in Ref. [28] to analyze our data. In Figure 2d, we plot σ_{SH}^* as a function of the rescaled thickness d_0 (the red circles) which uses 57.5 $\mu\Omega$ cm, the average resistivity of the 4 nm Pd_{0.25}Pt_{0.75} film, as the constant reference resistivity (ρ_{xx0}). Using $G^{\uparrow} \approx 6 \times 10^{14} \Omega^{-1} \text{m}^{-2}$ as an approximation as calculated for Pt/Co interfaces,[29] the best fit of σ_{SH}^* vs d_0 to the above Equation gives $\sigma_{\text{SH}} \approx (1.05 \pm 0.02) \times 10^6 \hbar/2e \Omega^{-1} \text{m}^{-1}$, $\lambda_s \approx 1.95 \pm 0.12$ nm (for 4 nm thickness), and T_{int} of 0.55. Accordingly, the internal θ_{SH} for 4 nm Pd_{0.25}Pt_{0.75} is determined to be > 0.47 after the SBF correction. From these results we find $1/\lambda_s \rho_{xx}$ for Pd_{0.25}Pt_{0.75} to be $\approx 0.89 \times 10^{15} \Omega^{-1} \text{m}^{-2}$, which is slightly larger than $0.71 \times 10^{15} \Omega^{-1} \text{m}^{-2}$ for Au_{0.25}Pt_{0.75} but considerably lower than $1.3 \times 10^{15} \Omega^{-1} \text{m}^{-2}$ obtained for Pt from a similar Pt thickness dependent study.[28] The relatively low spin conductance of Pd_{0.25}Pt_{0.75} is advantageous for reducing SBF at Pd_{0.25}Pt_{0.75} /FM interfaces. We also note that the large value for σ_{SH} is perhaps still a lower bound as it assumes an ideal Pd_{1-x}Pt_x/Co interface and does not take into account any SML induced by interfacial spin-orbit scattering. This lower-bound spin Hall conductivity of $\sim 1.1 \times 10^6 \hbar/2e \Omega^{-1} \text{m}^{-1}$ is substantially larger than $5.9 \times 10^5 \hbar/2e \Omega^{-1} \text{m}^{-1}$ of pure Pt [28] and $7.0 \times 10^5 \hbar/2e \Omega^{-1} \text{m}^{-1}$ for the Au_{0.25}Pt_{0.75} alloy[14], which indicates a significant enhancement in the spin Hall conductivity that warrant future theoretical efforts.

2.4. Strong and tunable interfacial DMI

Since the interfacial DMI strength is an important factor in many SOT phenomena and applications,[3-5] we quantitatively determined the interfacial DMI in Pd_{1-x}Pt_x 4/Fe_{0.6}Co_{0.2}B_{0.2} 2.6 bilayers by measuring the DMI-induced frequency difference (Δf_{DM}) between counter-propagating Damon-Eshbach spin

waves using BLS. Figure 3a shows the BLS measurement geometry, where a magnetic field $H = 1700$ Oe was applied along the x direction to align the magnetization of the FM layer. The total in-plane momentum is conserved during the scattering process. The anti-Stokes (Stokes) peaks in BLS spectra correspond to the annihilation (creation) of magnons with a wave-vector $k = \pm 4\pi\sin\theta/\lambda$, where θ is the light incident angle w.r.t. the film normal, and $\lambda = 532$ nm is the laser wavelength. In Figure 3b we plot Δf_{DM} as a function of k for different composition x . Here Δf_{DM} is the frequency difference of the $\pm k$ peaks and averaged for $\pm H$ (see more details in ref. [30]), as can be seen from the representative BLS spectrum in Figure 3c ($|k| = 9.6 \mu\text{m}^{-1}$, $H = 1700$ Oe, $x = 1$). The linear relation between Δf_{DM} and k for each x agrees with the expected relation $\Delta f_{\text{DM}} \approx (2\gamma/\pi\mu_0 M_s) D k$,^[31,32] where $\gamma \approx 176$ GHz/T is the gyromagnetic ratio and D is the volume-averaged (volumetric) DMI constant over the FM thickness. As shown in Figure 3d, with increasing x , D was tuned by a factor of ~ 5 , i.e. from -0.57 to -0.12 erg/cm². This strong tunability of interfacial DMI is mainly attributed to the variation of the SOC strength at the Pd_{1-x}Pt_x/Fe_{0.6}Co_{0.2}B_{0.2} interface as indicated by the linear relation between D and the interfacial magnetic anisotropy energy density (K_s) as determined from Fe_{0.6}Co_{0.2}B_{0.2} thickness dependent anisotropy studies using spin-torque ferromagnetic resonance (see Figure 3e and Figure S4). We interpret the intercept of the linear K_s - D fit as representing the contribution of the Fe_{0.6}Co_{0.2}B_{0.2}/MgO interface to the overall interfacial anisotropy energy density, i.e K_s (MgO) acc to the ov^2 for these as-grown/unannealed samples, while $K_s - K_s$ (MgO) is the contribution from the Pd_{1-x}Pt_x/Fe_{0.6}Co_{0.2}B_{0.2} interface and is an indicator of the interfacial SOC strength. Taking into account the inverse dependence of D on FM thickness t due to the volume averaging effect during BLS measurement, the total DMI strength for HM/Fe_{0.6}Co_{0.2}B_{0.2} interface can be estimated as $D_s = Dt$. For the Pd_{1-x}Pt_x/Fe_{0.6}Co_{0.2}B_{0.2} interfaces, D_s changes from -1.47×10^{-7} erg/cm at $x = 1$ to -0.30×10^{-7} erg/cm at $x = 0$. We note first that the DMI for our Pd_{1-x}Pt_x/Fe_{0.6}Co_{0.2}B_{0.2} interface is very strong compared with those for Ta (or W) / Fe_{0.6}Co_{0.2}B_{0.2} systems,^[30] i.e. D_s (Ta) = 0.36×10^{-8} erg/cm and D_s (W) = 0.73×10^{-8} erg/cm. Secondly, the Pd_{1-x}Pt_x composition enables a rather significant tunability of D_s because it is equivalent to a change from 8.3 (4.1) to 40.8 (20.1) times that of Ta (W)/Fe_{0.6}Co_{0.2}B_{0.2}

systems.^[32] The large amplitude of the DMI and its tunability ($\geq 3\times$) for $x \geq 0.5$ where $\zeta_{\text{DL}} \geq 0.2$, make Pd_{1-x}Pt_x especially intriguing for developing new chiral spintronic devices and for exploring new DMI effects on the performance of skyrmion, chiral domain wall devices, and micromagnetics during SOT magnetization switching. The quite different composition dependence of the interfacial DMI strength and damping-like SOT further confirms that the physical source of the observed strong SOTs in the Pd_{1-x}Pt_x/FM systems is dominated by the *bulk* SHE other than the *interfacial* SOC. Note that while the interfacial DMI is mainly determined by the *interfacial* SOC that is sensitive to the short-range ordering at the interface,^[10] the intrinsic bulk SHE is determined by the *bulk* SOC-rated topology of the band structure of the HMs.^[13]

2.5. High energy efficiency in spin-torque applications

We finally emphasize that the low ρ_{xx} and giant ζ_{DL} make Pd_{0.25}Pt_{0.75} advantageous for SOT research and technological applications with metallic FMs. As a simple example, we first show in Figure 4a that damping-like SOT generated by the SHE of a 4 nm Pd_{0.25}Pt_{0.75} can switch the magnetization of a Co 0.64 layer (with an effective PMA field of 7.7 kOe and coercivity of 0.44 kOe) with a dc current of ~ 4.8 mA (corresponding to $j_e = 2.2 \times 10^7$ A/cm² in the Pd_{0.25}Pt_{0.75} layer) and a bias field $H_x = \pm 100$ Oe applied along the current direction. This reaffirms the giant ζ_{DL} of Pd_{0.25}Pt_{0.75}. To better illustrate the advantage of Pd_{0.25}Pt_{0.75}, in Table I we compare the parameters that are most important for SOT applications, i.e. ζ_{DL} , ρ_{xx} , and σ_{SH}^* , for the various strong spin Hall materials. In Figure 4b and Table 1, we further compare the calculated write power consumption (P) for a typical in-plane magnetized SOT-MRAM device, which currently is of the most technological promise for very fast (~ 200 ps), low-current density, low-error rate,^[7] and field-free switching,^[33] based on these spin Hall materials by taking into consideration current shunting into the FeCoB free layer (see Supporting Information). Here we used a $600 \times 300 \times 4$ nm² spin Hall channel, a $190 \times 30 \times 1.8$ nm³ FeCoB free layer (resistivity ≈ 130 $\mu\Omega$ cm) and the parallel resistor model for the illustrative calculation (Supporting Information).

The power consumption for this modeled Pd_{0.25}Pt_{0.75}-based MRAM device is 320%, 50% and 20% smaller than low-resistivity Pt (20 μΩ cm)^[15], high-resistivity Pt (51 μΩ cm), and Au_{0.25}Pt_{0.75}. We note that ζ_{DL} of 0.2 for the high-resistivity pure Pt is the highest among the reported Pt values. The Pd_{0.25}Pt_{0.75}-based MRAM device is 8 and 23 times smaller than those based on β -W (300 μΩ cm),^[8] and β -Ta (190 μΩ cm),^[6] respectively. An MRAM device based on a magnetic tunnel junction with metallic ferromagnetic electrodes in combination with a Pd_{0.25}Pt_{0.75} spin Hall channel is estimated to be markedly more efficient in energy than those that might utilize the topological insulators Bi₂Se₃ (ζ_{DL} =3.5),^[34] (Bi,Se)₂Te₃ (ζ_{DL} =0.4),^[9] and Bi_xSe_{1-x} (ζ_{DL} =18.6),^[35] mainly because the colossal resistivity of the topological insulators results in very strong current shunting into the free layer and giant energy consumption in the channel. The small resistivity also makes Pd_{0.25}Pt_{0.75} more compelling than Au_{0.25}Pt_{0.75}^[14] for certain device applications, e.g. cryogenic computing, where the transistor circuits require a small write impedance for magnetic memory devices.^[36] Moreover, Pd_{0.25}Pt_{0.75} is compatible with both sputtering techniques and the use of Si substrates, which are preferable for integration technology. Therefore, the combination of the giant ζ_{DL} , the low ρ_{xx} , and the compatibility with microelectronics manufacturing technology makes Pd_{0.25}Pt_{0.75} a particularly attractive spin Hall material for the generation and detection of spin currents in spintronic devices.

3. Conclusions

We have established via direct SOT measurements a strong spin Hall material Pd_{0.25}Pt_{0.75} which has a giant internal spin Hall ratio of > 0.47 (yielding $\zeta_{DL} \approx 0.26$ for its bilayers with either Co or Fe_{0.6}Co_{0.2}B_{0.2}), spin Hall conductivity of > $1.1 \times 10^6 \hbar/2e \Omega^{-1}m^{-1}$, spin conductance $1/\lambda_s \rho_{xx}$ of $0.89 \times 10^{15} \Omega^{-1}m^{-2}$, and a relatively low ρ_{xx} of $\sim 57.5 \mu\Omega \text{ cm}$ (at 4 nm thickness). Particularly, this giant SHE and low ρ_{xx} make Pd_{0.25}Pt_{0.75} more energy-efficient for manipulating metallic magnetic devices than the other HMs (W, Ta, Pt, and Au_{0.25}Pt_{0.75}) and the topological insulators Bi_xSe_{1-x}, Bi₂Se₃ and (Bi,Se)₂Te₃. We also find the interfacial DMI at Pd_{1-x}Pt_x/Fe_{0.6}Co_{0.2}B_{0.2} interfaces is very strong and also widely tunable ($\times 5$) by Pt concentration x ; especially for $x \geq 0.5$ where $\zeta_{DL} \geq 0.2$, the interfacial DMI can be

tuned by a factor of 3. Our findings provide a highly efficient spin Hall material system that simultaneously combines a giant SHE, low resistivity, strong and tunable DMI, with excellent processing compatibility for device integration, for developing new efficient SOT-driven magnetic memories and chiral (skyrmion and chiral domain walls) spintronic devices.

4. Experimental Section

Sample growth and characterizations. The magnetic bilayers of $\text{Pd}_{1-x}\text{Pt}_x$ d/Co or $\text{Fe}_{0.6}\text{Co}_{0.2}\text{B}_{0.2}$ t with different Pt concentration ($x = 0, 0.25, 0.5, 0.75, \text{ and } 1$) were sputter deposited at room temperature on oxidized Si substrates and capped with MgO 2/Ta 1.5 protective layers where the Ta layer was fully oxidized upon exposure to the atmosphere. A seed layer of Ta 1 was grown prior to the co-sputtering of $\text{Pd}_{1-x}\text{Pt}_x$ layer in order to improve the adhesion and smoothness of the magnetic bilayers. The saturation magnetization of each sample was measured by a standard vibrating sample magnetometer embedded in a Quantum Design physical properties measurement system. A Rigaku Smartlab x-ray diffractometer was introduced to characterize the structure.

Device fabrication and measurement. The stacks were patterned into $5 \times 60 \mu\text{m}^2$ Hall bars by photolithography and ion milling for harmonic response measurements. A lock-in amplifier is introduced to source a 4 V sinusoidal voltage onto the Hall bar along the x axis (corresponding to an alternating electrical field of constant magnitude $E \approx 66.7 \text{ kV/m}$) and to detect the in-phase first and out-of-phase second harmonic Hall voltages. The current switching measurements were performed with a Yokogawa 76541 current source and a Keithley 2000 voltage meter.

Supporting Information

Supporting Information is available from the Wiley Online Library or from the author.

Acknowledgements

This work was supported in part by the Office of Naval Research, by the NSF MRSEC program (DMR-1719875) through the Cornell Center for Materials Research, and by the Office of the Director of National Intelligence (ODNI), Intelligence Advanced Research Projects Activity (IARPA), via contract W911NF-14-C0089. The views and conclusions contained herein are those of the authors and should not be interpreted as necessarily representing the official policies or endorsements, either expressed or implied, of the ODNI, IARPA, or the U.S. Government. The U.S. Government is authorized to reproduce and distribute reprints for Governmental purposes notwithstanding any copyright annotation thereon. The DMI measurement performed at UT-Austin was supported by SHINES, an Energy Frontier Research Center funded by the U.S. Department of Energy (DoE), Office of Science, Basic Energy Science (BES) under award # DE-SC0012670. The devices were fabricated in part at the Cornell NanoScale Facility, an NNCI member supported by NSF Grant ECCS-1542081.

Conflict of Interest

The authors declare no conflict of interest.

Key words: spin-orbit torque, spin Hall conductivity, spin Hall effect, Dzyaloshinskii-Moriya interaction

References

- [1] V. E. Demidov, S. Urazhdin, H. Ulrichs, V. Tiberkevich, A. Slavin, D. Baither, G. Schmitz, S. O. Demokritov, *Nat. Mater.* **2012**, 11, 1028.
- [2] Y. Wu, M. Elyasi, X. Qiu, M. Chen, Y. Liu, L. Ke, H. Yang, *Adv. Mater.* **2017**, 29, 1603031.
- [3] W. Jiang, P. Upadhyaya, W. Zhang, G. Yu, M. B. Jungfleisch, F. Y. Fradin, J. E. Pearson, Y. Tserkovnyak, K. L. Wang, O. Heinonen, S. G. E. Velthuis, A. Hoffmann, *Science* **2015**, 349, 283-286.

- [4] P. P. J. Haazen, E. Muré, J. H. Franken, R. Lavrijsen, H. J. M. Swagten, B. Koopmans, *Nat. Mater.* **2013**, 12, 299.
- [5] O. J. Lee, L. Q. Liu, C. F. Pai, Y. Li, H. W. Tseng, P. G. Gowtham, J. P. Park, D. C. Ralph, R. A. Buhrman, *Phys. Rev. B* **2014**, 89, 024418.
- [6] L. Liu, C.-F. Pai, Y. Li, H. W. Tseng, D. C. Ralph, R. A. Buhrman, *Science*, **2012**, 336, 555.
- [7] S. Shi, Y. Ou, S.V. Aradhya, D. C. Ralph, R. A. Buhrman, *Phys. Rev. Applied* **2018**, 9, 011002.
- [8] C.-F. Pai, L. Liu, Y. Li, H. W. Tseng, D. C. Ralph, R. A. Buhrman, *Appl. Phys. Lett.* **2012**, 101, 122404.
- [9] J. Han, A. Richardella, S. A. Siddiqui, J. Finley, N. Samarth, and L. Liu, *Phys. Rev. Lett.* **2017**, 119, 077702.
- [10] H. Yang, A. Thiaville, S. Rohart, A. Fert, and M. Chshiev, *Phys. Rev. Lett.* **2015**, 115, 267210.
- [11] G. E. Rowlands, S. V. Aradhya, S. Shi, E. H. Yandel, J. Oh, D. C. Ralph, R. A. Buhrman, *Appl. Phys. Lett.* **2017**, 110, 122402.
- [12] M. Cubukcu, J. Sampaio, K. Bouzehouane, D. Apalkov, A. V. Khvalkovskiy, V. Cros, N. Reyren, *Phys. Rev. B* **2016**, 93, 020401(R).
- [13] E. Sagasta, Y. Omori, M. Isasa, M. Gradhand, L. E. Hueso, Y. Niimi, Y. Otani, F. Casanova, *Phys. Rev. B* **2016**, 94, 060412(R).
- [14] L. Zhu, D. C. Ralph, and R. A. Buhrman, *Phys. Rev. Applied* **2018**, 10, 031001.
- [15] L. Liu, T. Moriyama, D. C. Ralph, R. A. Buhrman, *Phys. Rev. Lett.* **2011**, 106, 036601.
- [16] C.-F. Pai, Y. Ou, L. H. Vilela-Leao, D. C. Ralph, R. A. Buhrman, *Phys. Rev. B* **2015**, 92, 064426.
- [17] M.-H. Nguyen, M. Zhao, D.C. Ralph, R. A. Buhrman, *Appl. Phys. Lett.* **2016**, 108, 242407.
- [18] J. W. Lee, Y.-W. Oh, S.-Y. Park, A. I. Figueroa, G. van der Laan, G. Go, K.-J. Lee, B.-G. Park, *Phys. Rev. B* **2017**, 96, 064405.
- [19] C. L. Canedy, X.W. Li, G. Xiao, *Phys. Rev. B* **2000**, 62, 508-519.
- [20] T. A. Peterson, A. P. McFadden, C. J. Palmstrøm, P. A. Crowell, *Phys. Rev. B* **2018**, 97, 020403(R).

- [21] L. Zhu, D. C. Ralph, and R. A. Buhrman, *Phys. Rev. B* **2018**, 98, 134406.
- [22] M. Hayashi, J. Kim, M. Yamanouchi, H. Ohno, *Phys. Rev. B* **2014**, 89, 144425.
- [23] C. O. Avci, K. Garello, M. Gabureac, A. Ghosh, A. Fuhrer, S. F. Alvarado, P. Gambardella, *Phys. Rev. B* **2014**, 90, 224427.
- [24] J.-C. Rojas-Sánchez, N. Reyren, P. Laczkowski, W. Savero, J.-P. Attané, C. Deranlot, M. Jamet, J.-M. George, L. Vila, H. Jaffrès, *Phys. Rev. Lett.* **2014**, 112, 106602.
- [25] A. Ghosh, K. Garello, C. O. Avci, M. Gabureac, P. Gambardella, *Phys. Rev. Appl.* **2017**, 7, 014004.
- [26] X. Zhou, M. Tang, X. L. Fan, X. P. Qiu, and S. M. Zhou, *Phys. Rev. B* **2016**, 94, 144427.
- [27] L. Ma, H.-A. Zhou, L. Wang, X.-L. Fan, W.-J. Fan, D.S. Xue, K. Xia, Z. Wang, R.-Q. Wu, G.-Y. Guo, L. Sun, X. Wang, X.-M. Cheng, S.-M. Zhou, *Adv. Electron. Mater.* **2016**, 2, 1600112.
- [28] M.-H. Nguyen, D. C. Ralph, R. A. Buhrman, *Phys. Rev. Lett.* **2016**, 116, 126601.
- [29] P. M. Haney, H.-W. Lee, K.-J. Lee, A. Manchon, M. D. Stiles, *Phys. Rev. B* **2013**, 87, 174411.
- [30] X. Ma, G. Yu, C. Tang, X. Li, C. He, J. Shi, K. L. Wang, X. Li, *Phys. Rev. Lett.* **2018**, 120, 157204.
- [31] J.-H. Moon, S.-M. Seo, K.-J. Lee, K.-W. Kim, J. Ryu, H.-W. Lee, R. D. McMichael, M. D. Stiles, *Phys. Rev. B* **2013**, 88, 184404.
- [32] H. T. Nembach, J. M. Shaw, M. Weiler, E. Jué, T. J. Silva, *Nat. Phys.* **2015**, 11, 825.
- [33] S. Fukami, T. Anekawa, C. Zhang, H. Ohno, *Nat. Nanotech.* **2016**, 11, 621–625.
- [34] A. R. Mellnik, J. S. Lee, A. Richardella, J. L. Grab, P. J. Mintun, M. H. Fischer, A. Vaezi, A. Manchon, E. -A. Kim, N. Samarth, D. C. Ralph, *Nature* **2014**, 511, 499-451.
- [35] M. DC, R. Grassi, J.-Y. Chen, M. Jamali, D. R. Hickey, D. Zhang, Z. Zhao, H. Li, P. Quarterman, Y. Lv, M. Li, A. Manchon, K. A. Mkhoyan, T. Low, J.-P. Wang, *Nat. Mater.* **2018**, DOI: 0.1038/s41563-018-0136-z.
- [36] D.S. Holmes, A. L. Ripple, M. A. Manheiner, *IEEE Trans. Appl. Supercond.* **2013**, 23, 1701610.

Table I. Comparison of ζ_{DL} , ρ_{xx} , σ_{SH}^* , and normalized power consumption P for various strong spin current generators (thickness = 4 nm).

	ζ_{DL}	ρ_{xx} ($\mu\Omega$ cm)	σ_{SH}^* ($10^5 \hbar/2e \Omega^{-1}m^{-1}$)	P	Ref.
Pd _{0.25} Pt _{0.75}	0.26	57.5	4.5	0.68	This work
Au _{0.25} Pt _{0.75}	0.3	83	3.6	0.82	Zhu <i>et al</i> [14]
Pt (high- ρ_{xx})	0.20	51	3.9	1	This work
Bi ₂ Se ₃	3.5	1755	2.0	2.1	Mellnik <i>et al</i> [34]
Pt (low- ρ_{xx})	0.07	20	3.5	2.8	Liu <i>et al</i> [15]
β -W	0.3	300	1.0	5.7	Pai <i>et al</i> [8]
β -Ta	0.12	190	0.63	16.7	Liu <i>et al</i> [6]
Bi _x Se _{1-x}	18.6	13000	1.4	20	DC <i>et al</i> [35]
(Bi,Se) ₂ Te ₃	0.4	4020	0.1	1474	Han <i>et al</i> [9]

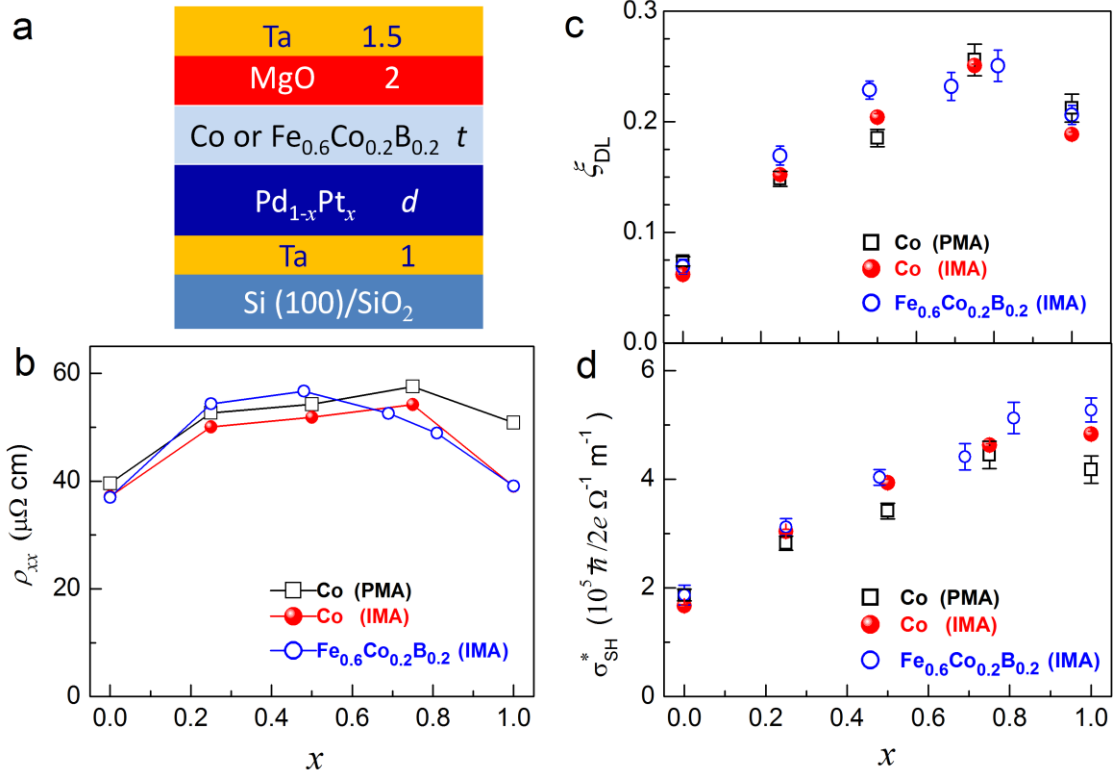


Figure 1. a) Schematic depiction of the magnetic stacks. x dependence of b) Pd_{1-x}Pt_x resistivity (ρ_{xx}), c) ζ_{DL} and σ_{SH}^* for 4 nm Pd_{1-x}Pt_x using Co and Fe_{0.6}Co_{0.2}B_{0.2} as FM detectors in the SOT measurements.

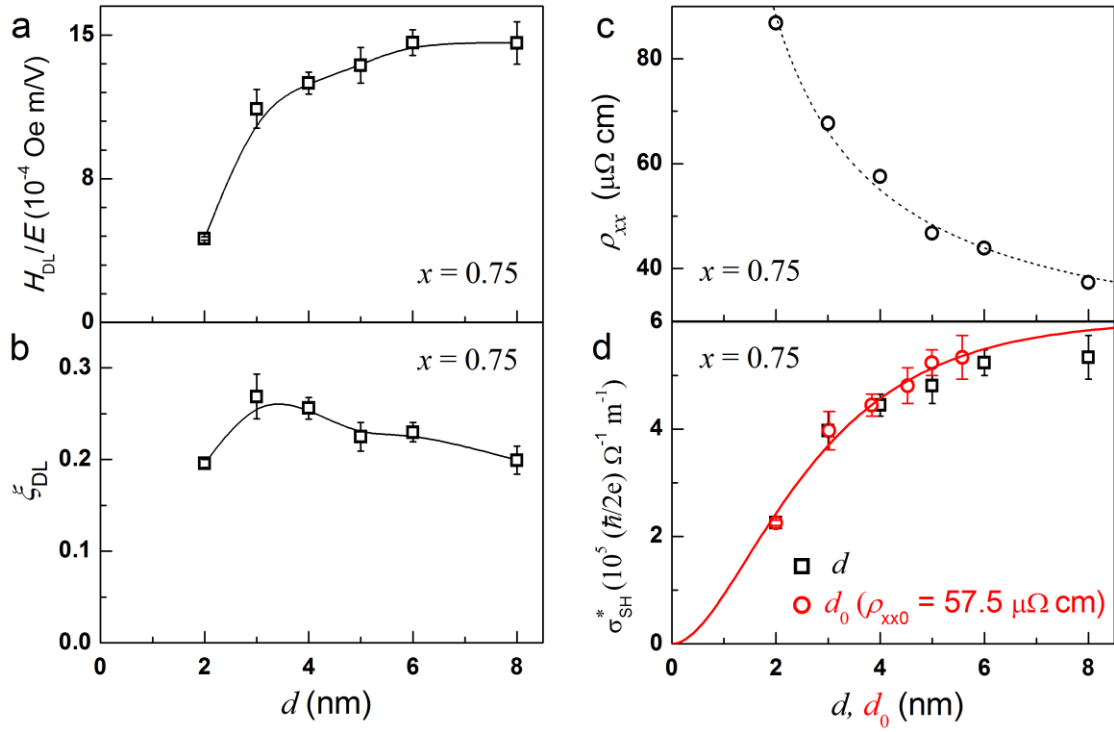


Figure 2. $\text{Pd}_{0.25}\text{Pt}_{0.75}$ thickness (d) dependence of a) H_{DL}/E , b) ζ_{DL} , and c) ρ_{xx} ; d) σ_{SH}^* plotted as a function of d (black squares) and the rescaled effective thickness (d_0 , red circles). The solid curve donates the best $\sigma_{\text{SH}}^* - d_0$ fit. In d), d_0 was rescaled with the resistivity of the 4 nm $\text{Pd}_{0.25}\text{Pt}_{0.75}$ film ($\rho_{xx0} = 57.5 \mu\Omega$ cm).

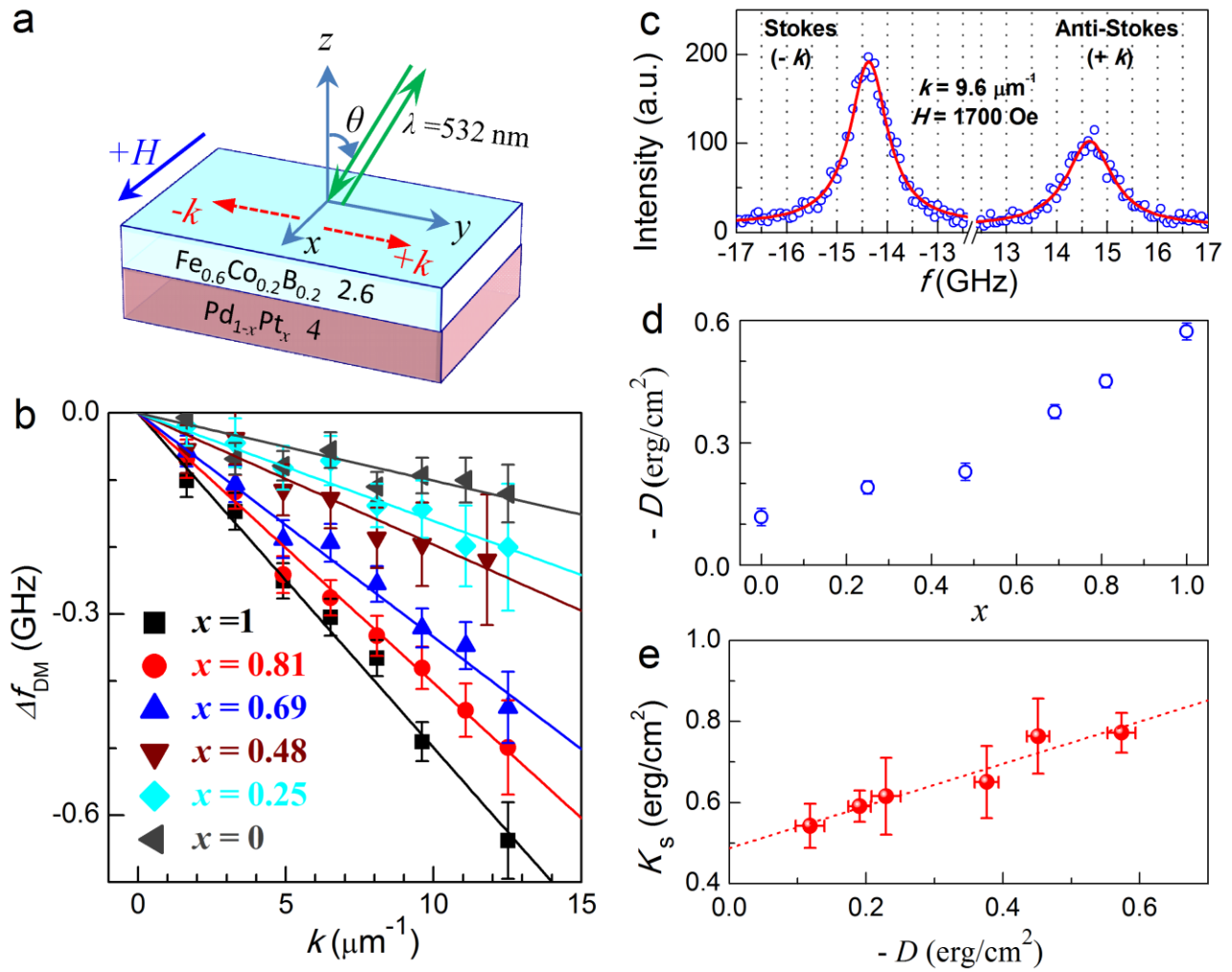


Figure 3. a) BLS measurement geometry; b) k dependence of Δf_{DM} ; c) BLS spectra at $k = 9.6 \mu\text{m}^{-1}$ and $H = 1700 \text{ Oe}$ ($x = 1$); and d) $-D$, and e) K_s vs $-D$ for $\text{Pd}_{1-x}\text{Pt}_x \text{ 4} / \text{Fe}_{0.6}\text{Co}_{0.2}\text{B}_{0.2} \text{ 2.6}$ bilayers with different x . The red solid curves in c) represent fits to the Lorentzian function; the dashed line in e) refers to the best linear fit.

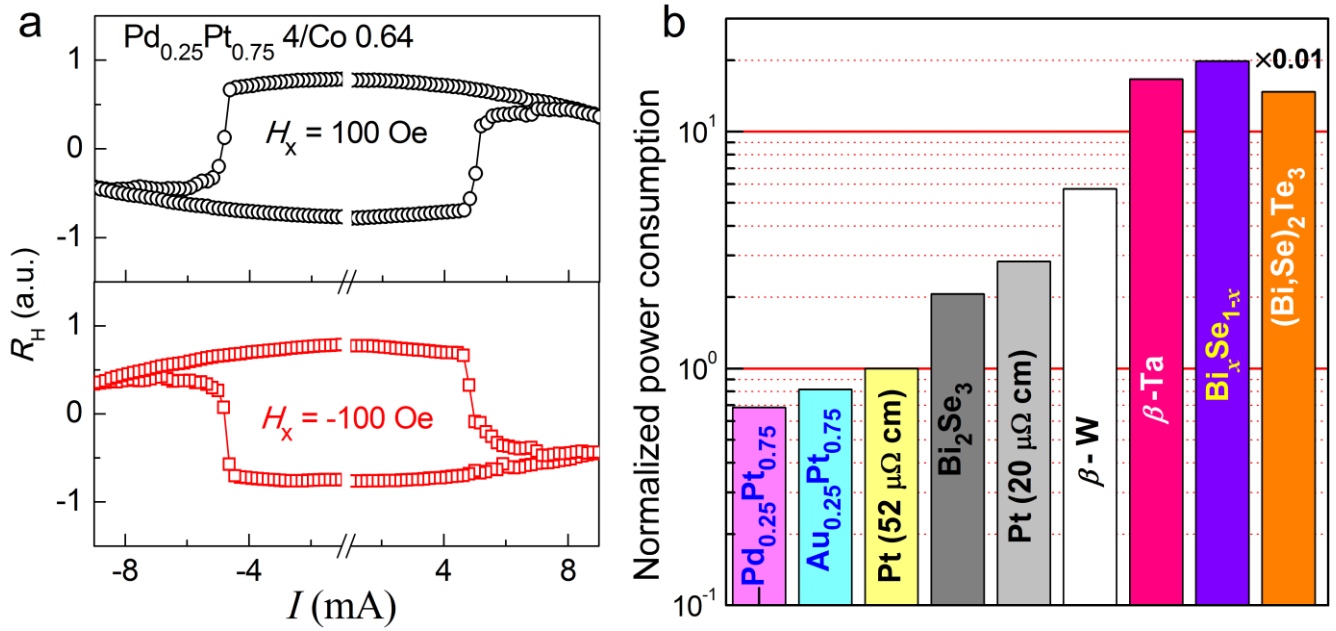


Figure 4. a) Deterministic current-induced magnetization switching in Pd_{0.25}Pt_{0.75} 4 nm/Co 0.64 nm bilayers (effective PMA field ≈ 7.7 kOe and coercivity ≈ 0.44 kOe) with a bias field $H_x = \pm 100$ Oe along current direction; b) Power consumption of normalized SOT-MRAM application for different spin Hall channel materials listed in Table I.

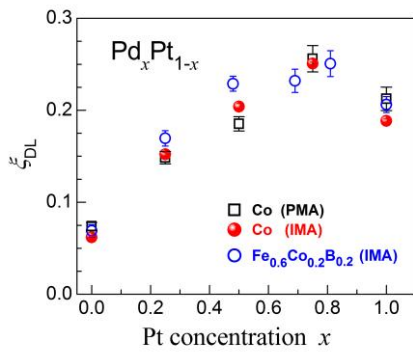
Spin-orbit torque (SOT) operations are currently energy inefficient due to a low damping-like SOT efficiency and/or the very high resistivity of the spin Hall materials. This work establishes a very effective spin current generator $\text{Pd}_{1-x}\text{Pt}_x$ that combines a notably high energy efficiency with a very strong and tunable DMI for advanced chiral spintronics and spin torque applications.

Key words: spin-orbit torque, spin Hall conductivity, spin Hall effect, Dzyaloshinskii-Moriya interaction

Authors: L. J. Zhu,* K. Sobotkiewich, X. Ma, X. Li, D. C. Ralph, R. A. Buhrman*

Titles: Strong damping-like spin-orbit torque and tunable Dzyaloshinskii-Moriya interaction generated by low-resistivity $\text{Pd}_{1-x}\text{Pt}_x$ alloys

ToC figure



Supporting Information

Strong and tunable anti-damping spin-orbit torque and Dzyaloshinskii-Moriya interaction generated by low-resistivity Pd_{1-x}Pt_x alloys

Lijun Zhu,¹ Kemal Sobotkiewich,² Xin Ma,² Xiaoqin Li,² Daniel. C. Ralph,^{1,3} Robert A. Buhrman¹

1. Cornell University, Ithaca, NY 14850, USA

2. Department of Physics, Center for Complex Quantum Systems, The University of Texas at Austin, Austin, Texas 78712, USA

3. Kavli Institute at Cornell, Ithaca, New York 14853, USA

A. X-Ray diffraction measurements

B. Out-of-plane Harmonics response measurements

C. In-plane harmonics response measurements

D. Determination of interfacial magnetic anisotropy energy density from FM thickness dependence study

E. Calculation of power consumption of a SOT-MRAM device

A. X-Ray diffraction measurements

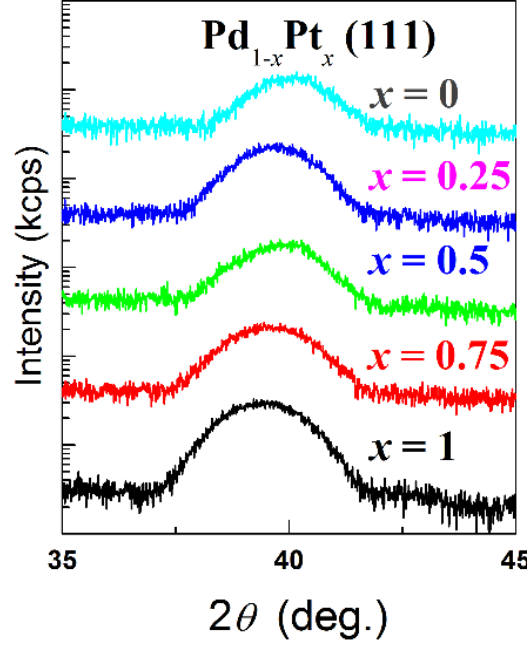


Figure S1. X-ray diffraction θ - 2θ patterns for Pd_{1-x}Pt_x 4/Co t ($t = 0.75$ for $x = 1$ and 0.64 for $x \leq 0.75$) with different Pd_{1-x}Pt_x composition x .

B. Out-of-plane Harmonics response measurements

For harmonic response measurements, a lock-in amplifier was used to source a sinusoidal voltage ($V_{in} = 4$ V) onto the bar (length $L = 60$ μm) orientated along the x axis (see Figure S2(a)) and to detect the in-phase first and out-of-phase second harmonic Hall voltages, $V_{1\omega}$ and $V_{2\omega}$. As shown in Figure S2(b), the fairly square anomalous Hall voltage (V_{AH}) hysteresis loops of Pd_{1-x}Pt_x 4/Co 0.64 bilayers and the large coercivity of 250-500 Oe evidence the strong PMA of these samples, which allows us to obtain high-quality out-of-plane harmonic response data. The damping-like (H_{DL}) and field-like (H_{FL}) effective spin-torque field can be determined following $H_{DL(FL)} = -2 \frac{\partial V_{2\omega}}{\partial H_{x(y)}} / \frac{\partial^2 V_{1\omega}}{\partial^2 H_{x(y)}}$. We note that in analyzing our out-of-plane harmonics results we do not employ the so-called ‘‘planar Hall correction (PHC)’’ which was developed to account for any magnetoresistance effects in PMA HM/FM bilayers (the combination of anisotropic magnetoresistance in the FM and spin Hall magnetoresistance in the HM)^[1] So far, there have little discussion in the published literature about the ‘‘PHC problem’’ although, as far as we know, it has been noticed by some other groups experienced in the harmonic technique. We do note that recently M. Hayashi, the developer of this ‘‘PHC’’, has noted the existence of the

problem.^[2] Experimentally, this “PHC” is not of a concern when the HM/FM systems have very poor interfacial spin transparency and very small spin torques are exerted because in that case, the changes in the measured spin torques due to this “PHC” are boringly small. The “PHC” is also found not to be important for high-spin transparency HM/FM systems when the ratio of the planar Hall voltage (V_{PH}) and anomalous Hall voltage (V_{AH}), $\zeta = V_{PH}/V_{AH}$ is not larger than ~ 0.1 as this correction actually has negligible influence on the value of the damping-like effective spin torque field (efficiency). However when ζ approaches 0.5, this “PHC” gives an infinite change, which certainly indicates the invalidity of the “PHC” in that case. In fact, when ζ is larger than typically > 0.2 , we find this “correction” leads to larger numbers for the dampinglike spin-torque efficiency than it should be in all cases, in some cases to unphysical (sign reversal) values, that are in sharp disagreement with those values obtained from our other technique, i.e. the harmonic response measurements on the in-plane magnetized samples. Neglecting the PHC for the PMA samples gives results that are in close accord with the results from the IMA samples (see Figure 1c in the main text for a comparison of the dampinglike spin torque efficiencies from different techniques and different HM/FM systems). The clarifying of possible origins of this absence of magnetoresistance effects in the PMA harmonic measurements is beyond the scope of this paper and will be discussed elsewhere in detail. Here we show a few examples for the absence of such “PHC” in Table S1. The “PHC”, if applied, will give unreasonably larger dampinglike spin torque efficiency ζ_{DL} for the PMA Pt and Pd_{0.25}Pt_{0.75} samples, and unphysical sign change in case of PMA Pd samples. In all the cases, the tentative application of such “PHC” leads to fieldlike spin torque efficiency ζ_{FL} that is unphysical in magnitude and sign. We also see such invalidity (sign change) of “PHC” for β -W samples.

Table S1 Examples for the absence of the so-called “planar Hall correction”.

	$\zeta = V_{PH}/V_{AH}$	Out-of-plane harmonics No “PHC”		Out-of-plane harmonics With “PHC”		In-plane harmonics
		ζ_{DL}	ζ_{FL}	ζ_{DL}	ζ_{FL}	ζ_{DL}
Pt/Co	0.31	0.21	-0.049	0.30	0.14	0.19
Pd _{0.25} Pt _{0.75} /Co	0.28	0.26	-0.048	0.33	0.13	0.25
Pd/Co	0.56	0.07	-0.050	-0.1	-0.16	0.06

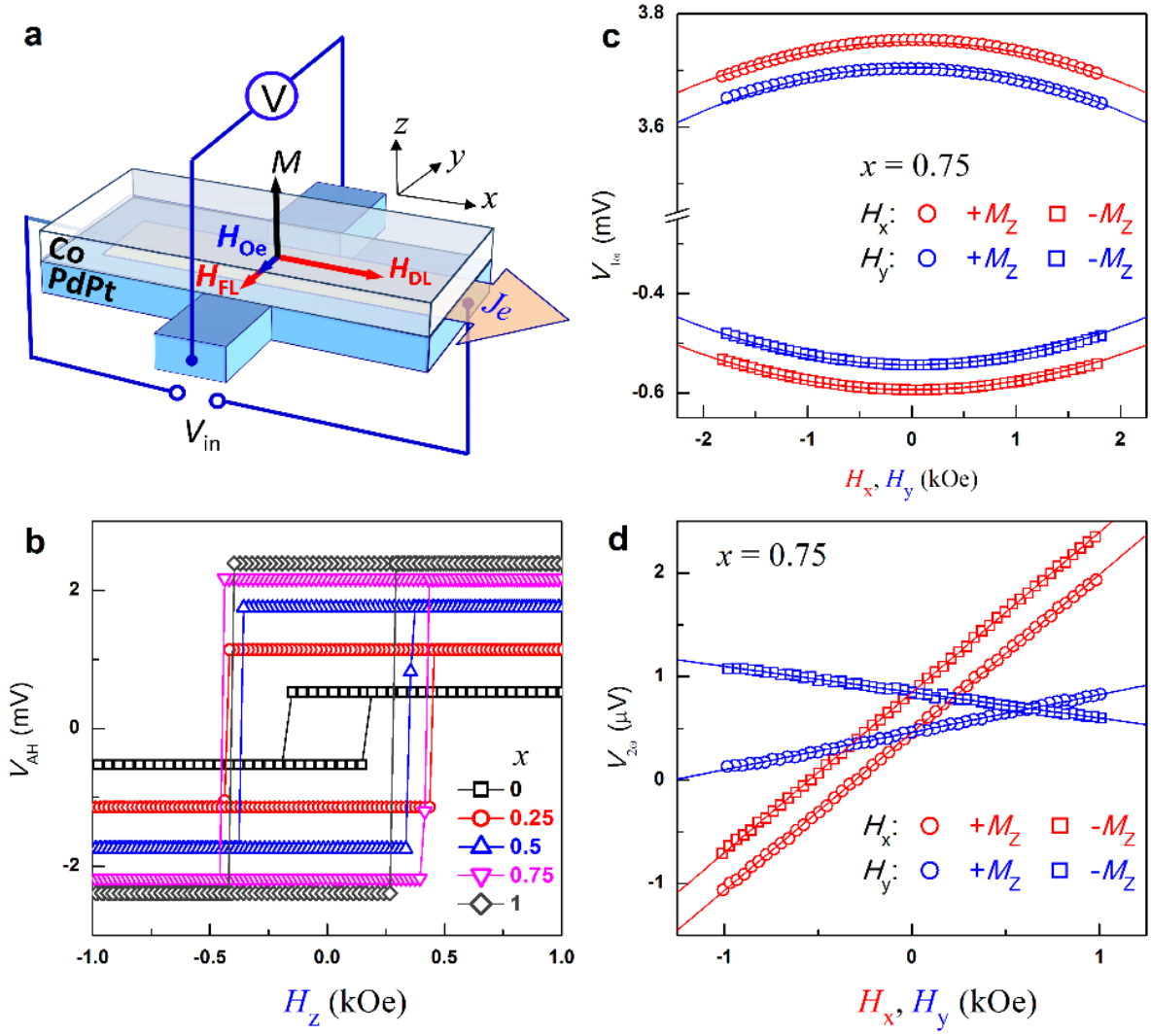


Figure S2. Out-of-plane harmonic response measurement. **a)** Schematic of the Hall bar devices and the measurement coordinate, a 4 V sinusoidal voltage was sourced onto the Hall bar along the x axis for all the harmonic response measurements; **b)** Anomalous Hall voltage hysteresis loops for different x ; **c).** The first ($V_{1\omega}$) and **d)** second ($V_{2\omega}$) harmonic voltages plotted as a function of in-plane fields H_x (red) and H_y (blue), respectively (for $x = 0.75$). For clarity, the H_y -dependent $V_{1\omega}$ data in **d)** are artificially shifted by ± 0.001 mV for $\mp M_z$, respectively.

C. In-plane harmonics response measurements

For in-plane magnetized HM/FM bilayer, the in-plane angle (φ) dependence of $V_{2\omega}$ is given by $V_{2\omega} = V_a \cos \varphi + V_p \cos \varphi \cos 2\varphi$, where $V_a = -V_{AH} H_{DL} / 2(H_{in} + H_k) + V_{ANE}$, and $V_p = -V_{PH} H_{FL} / 2H_{in}$ with V_{AH} , V_{ANE} , H_{in} , H_k , V_{PH} , H_{DL} , and H_{FL} being anomalous Hall voltage, anomalous Nernst effect, in-plane bias field, perpendicular anisotropy field, planar Hall voltage, damping-like effective spin torque field, and field-like effective spin torque field. φ dependence of $V_{1\omega}$ is given by $V_{1\omega} = V_{PH} \cos 2\varphi$, from which the planar Hall voltage V_{PH} can be determined. We separated the damping-like term V_a and the field-like term V_p

for each H_{in} and each x by fitting $V_{2\omega}$ data to $V_{2\omega} = V_a \cos \varphi + V_p \cos \varphi \cos 2\varphi$ (see Fig. S3(a)). The linear fits of V_a versus $-V_{AH}/2(H_{in}+H_k)$ and V_p versus $-V_{PH}/2H_{in}$ (see Fig. S3(b)) yield the values of H_{DL} and H_{FL} for $Pt_x(MgO)_{1-x}/Co$ bilayers. Here $V_a = -H_{DL}V_{AH}/2(H_k+H_{in}) + V_{ANE}$, $V_p = -V_{PH}H_{FL}/2H_{in}$ where V_{PH} , V_{ANE} , and H_{in} are the planar Hall voltage, the anomalous Nernst effect voltage, and the applied in-plane magnetic field, respectively.

Here we further discuss the thermoelectronic effects. For HM/FM bilayer, there could be a vertical thermal gradient generated due to the Joule heating and asymmetric thermal dissipation into the substrate and capping layer. This vertical thermal gradient can contribute a transverse voltage that scales with $\nabla T \times M$ via either anomalous Nernst effect (ANE) and longitudinal spin Seebeck effect (SEE). Here the symmetry of the longitudinal SEE is the same as that of the ANE signal, while the longitudinal SEE signal is generally negligible compared to the ANE signal ($V_{ANE} + V_{SEE} \approx V_{ANE}$).^[3] For perpendicularly magnetized bilayers, e.g. Pt/Co, the harmonic response voltages are not influenced by the thermal gradient as $\nabla T \times M = 0$. For in-plane harmonic response measurements, the signal contributions of ANE and SEE are subtracted by the linear fits of V_a versus $-V_{AH}/2(H_{in}+H_k)$ and V_p versus $-V_{PH}/2H_{in}$ yield the values of H_{DL} and H_{FL} for $Pt_x(MgO)_{1-x}/Co$ bilayers.

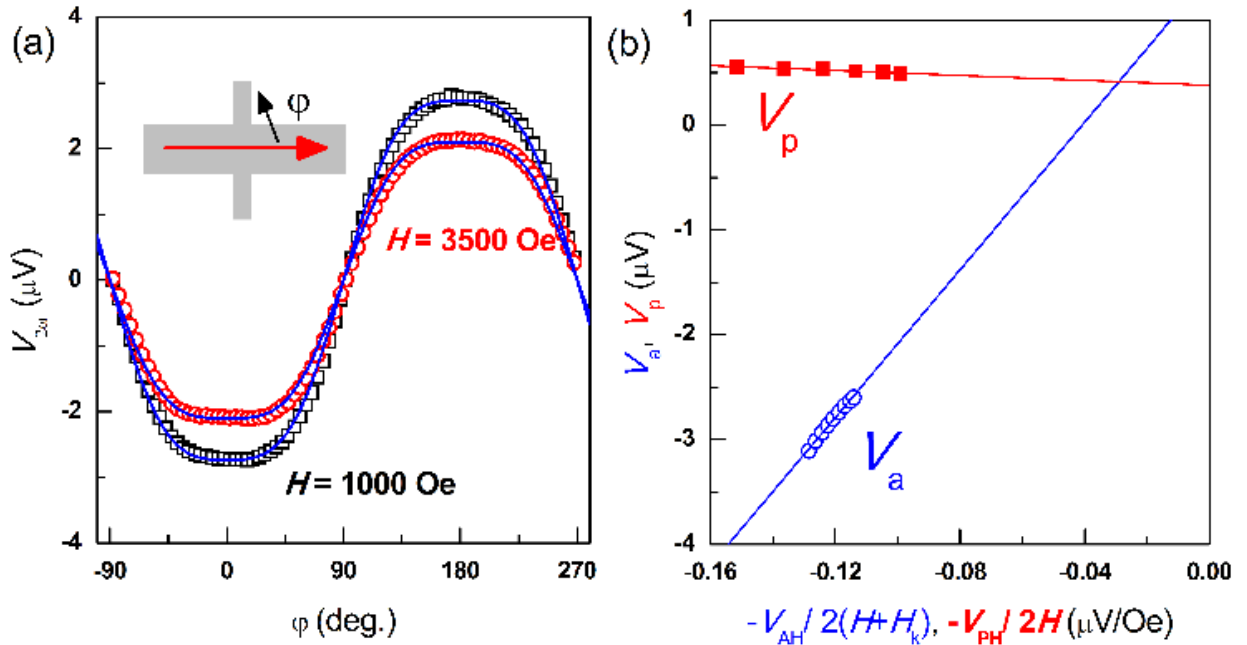


Figure S3. In-plane harmonic response measurement. **a)** In-plane angle (φ) dependence of $V_{2\omega}$ for the $Pd_{0.25}Pt_{0.75}/Fe_{0.6}Co_{0.2}B_{0.2}$ bilayer under in-plane bias fields with magnitudes of 1000 (blue) and 3500 Oe (red), the solid lines refer to the best fit to $V_{2\omega} = V_a \cos \varphi + V_p \cos \varphi \cos 2\varphi$, where $V_a = -H_{DL}V_{AH}/2(H_k+H_{in}) + V_{ANE}$, $V_p = -V_{PH}H_{FL}/2H_{in}$ with V_{PH} , V_{ANE} , and H_{in} are the planar Hall voltage, the anomalous Nernst effect voltage, and the applied in-plane magnetic field, respectively. **b)** V_a vs $-V_{AH}/2(H_k+H_{in})$ and V_p vs $-V_{PH}/2H_{in}$ for the $Pd_{0.25}Pt_{0.75}/Fe_{0.6}Co_{0.2}B_{0.2}$ bilayer, where V_a and V_p determined by fitting the φ dependence of $V_{2\omega}$. The slopes of the linear fits give H_{DL} and H_{FL} .

D. Determination of interfacial magnetic anisotropy energy density from FM thickness dependence study

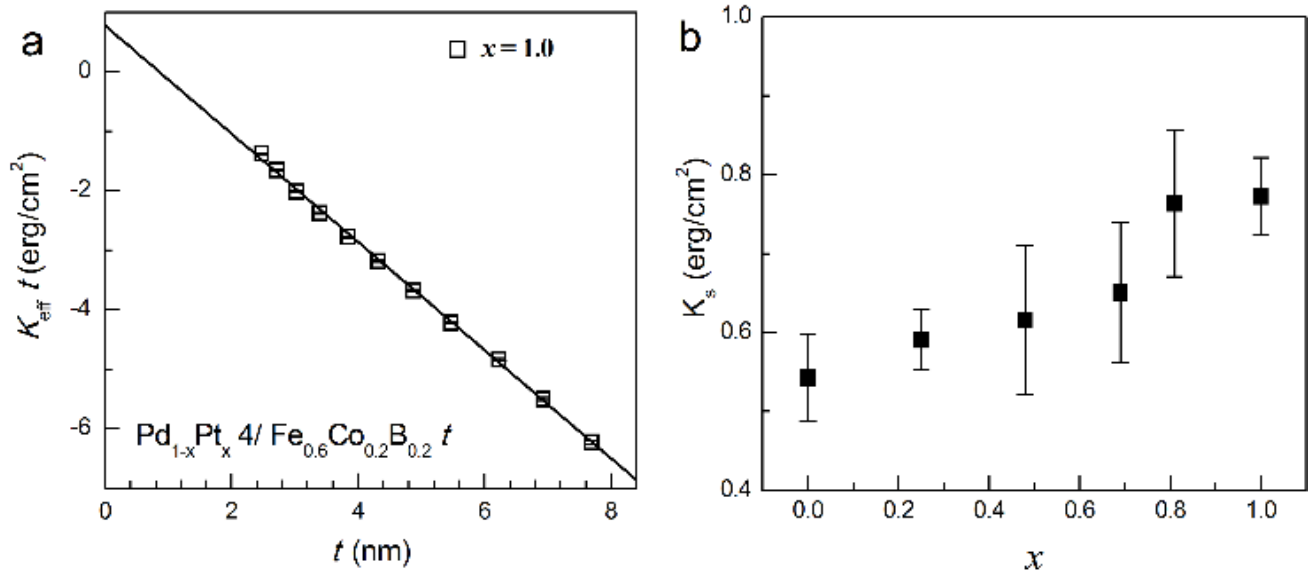


Figure S4| Determination of interfacial magnetic anisotropy energy density. a) $K_{\text{eff}} t$ vs t for Pt 4/ $\text{Fe}_{0.6}\text{Co}_{0.2}\text{B}_{0.2}$ t bilayers. Here $K_{\text{eff}} = -4\pi M_{\text{eff}} M_s/2$ is perpendicular anisotropy energy, and the effective magnetization $-4\pi M_{\text{eff}} = -4\pi M_s + 2 K_s/t$ and saturation magnetization M_s are determined by spin-torque ferromagnetic resonance and VSM, respectively; b) The interfacial magnetic anisotropy energy density K_s determined by the intercept of linear $K_{\text{eff}} t - t$ fits following $K_{\text{eff}} t = 2\pi M_s^2 t + K_s$.

E. Calculation of power consumption of a SOT-MRAM device

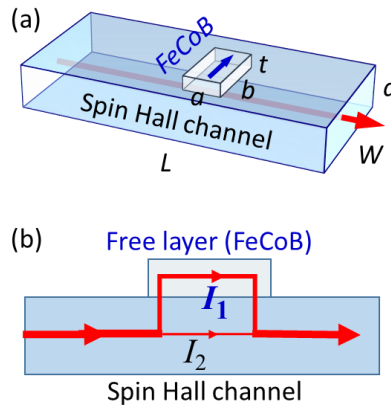


Figure S5. Schematics for a spin-orbit torque MRAM device. a) Dimension definitions. b) Current shunting into free layer.

Here we calculate the power efficiency of a model spin-orbit torque MRAM device consisting of a $400 \times 200 \times 4 \text{ nm}^3$ spin Hall channel and a $110 \times 30 \times 1.8 \text{ nm}^3$ FeCoB free layer (resistivity $\rho_{\text{FeCoB}} = 130 \mu\Omega \text{ cm}$) by taking into account the current shunting into the free layer. For convenience of discussion, we note the device dimensions as shown in Figure S5a: channel length $L = 400 \text{ nm}$, channel width $W = 200 \text{ nm}$, channel thickness $d = 4 \text{ nm}$; free layer “length” $a = 30 \text{ nm}$, free layer “width” $b = 110 \text{ nm}$, free layer thickness $t = 1.8 \text{ nm}$, free layer length $a = 30 \text{ nm}$, free layer width $b = 110 \text{ nm}$, and free layer thickness $t = 1.8 \text{ nm}$. Since $t \ll a$ and $t \ll b$, current spreading has a minimal influence and a parallel resistor model can be used. The total write current (I_{tot}) in the spin Hall channel is given by

$$I_{\text{tot}} = I_2 + I_1 = I_2 \left(1 + \frac{I_1}{I_2}\right) = I_2 \left(1 + \frac{\rho_{\text{HM}}}{\rho_{\text{FM}}} \frac{t a}{d W}\right) \quad (1)$$

where I_1 is the current shunted into the FeCoB free layer and I_2 is the “useful” current in the spin Hall channel that drives the magnetization switching (Figure S5b). ρ_{FM} and ρ_{HM} are resistivity of the free layer and heavy metal layers, respectively. According to macrospin model, which is found to work reasonably well for in-plane magnetized magnetic tunneling junctions, we have

$$I_2 = \frac{2e}{\hbar} \mu_0 M_s t_{\text{FM}} \alpha (H_c + 4\pi M_{\text{eff}} / 2) / \xi_{\text{DL}} \quad (2)$$

in which e , μ_0 , \hbar , α , H_c , M_{eff} , and ξ_{DL} are the elementary charge, the permeability of vacuum, the reduced Planck constant, the magnetic damping, the coercivity, the effective magnetization, the damping-like spin torque efficiency, respectively.

The power consumption is then given by:

$$P = I_1^2 \rho_{\text{FM}} \frac{a}{bt} + I_2^2 \rho_{\text{HM}} \frac{a}{Wd} + I_{\text{tot}}^2 \rho_{\text{HM}} \frac{L-a}{Wd} \quad (3)$$

-
1. M. Hayashi, J. Kim, M. Yamanouchi, and H. Ohno, Quantitative characterization of the spin-orbit torque using harmonic Hall voltage measurements, *Phys. Rev. B* 89, 144425 (2014).
 2. Y.-C. Lau and M. Hayashi, Spin torque efficiency of Ta, W, and Pt in metallic bilayers evaluated by harmonic Hall and spin Hall magnetoresistance measurements, *Jpn. J. Appl. Phys.* 56,0802B5 (2017).
 3. C. O. Avci, K. Garello, M. Gabureac, A. Ghosh, A. Fuhrer, S. F. Alvarado, and P. Gambardella, Interplay of spin-orbit torque and thermoelectric effects in ferromagnet/normal-metal bilayers, *Phys. Rev. B* 90, 224427 (2014).